First publ. in: Micromagnetism / ed.-in-chief: Helmut Kronmüller ... Chichester : Wiley, 2007, pp. 858-876
(= Handbook of magnetism and advanced magnetic materials ; 2)
The definitive version is available at www3.interscience.wiley.com

Classical Spin Models

Ulrich Nowak
University of York, York, UK

1 INTRODUCTION

Classical spin models bridge the gap between a full electronic description of a magnetic material and conventional micromagnetism where magnetic properties are calculated on the basis of a continuum theory for the energy of a system. While quantum effects are obviously neglected, classical spin models take into account the discrete nature of matter, so that they allow for an investigation of magnetic particles in the nanometer regime where a continuum theory would fail. The fact that magnetic structures are described on an atomic level makes it possible to investigate ferromagnets (FMs) as well as antiferromagnets (AFMs) or even heterostructures composed of both of them. Methods exist for the calculation of thermal equilibrium properties and, to some extent, also for nonequilibrium properties. Classical spin models are thus particularly suited to the study of thermal effects. On the other hand, numerical calculations with an atomic resolution are restricted to system sizes of the order of 10^7 spins so that only systems sizes of the order of some 10 nm can be treated numerically (at the moment). However, magnetic materials are controllable down to the nanometer scale, leading to a fundamental interest in the understanding of the magnetism of small ferromagnetic particles or heterostructures (Schneider and Blügel, 2005). This interest is even amplified by the broad variety of industrial applications in pure magnetic as well as spin electronic devices. For theoretical investigations numerical methods are thus desirable, especially methods that are capable of treating realistic magnetic model systems including heterostructures and the effects of thermal activation.

This chapter focuses on classical spin models, physical principles as well as numerical methods. Section 2 deals with the basics of classical spin Hamiltonians, thermal averages, and the equation of motion – the Landau–Lifshitz–Gilbert (LLG) equation. In Section 3 the two most established numerical methods in this context are discussed, namely Monte Carlo methods (Binder and Heermann, 1997) and Langevin dynamics simulations (Lyberatos and Chantrell, 1993). Special emphasis is laid on the relation between these different methods, which leads to time-quantified Monte Carlo methods (Nowak, Chantrell and Kennedy, 2000). Sections 4 and 5 are an introduction to two topics which are typical for a modeling within the framework of classical spin models, namely thermally activated switching in nanoparticles (Nowak, 2001) and exchange bias (EB) (Nogués and Schuller, 1999), an effect arising in compound systems of ferro- and antiferromagnetic materials. Section 6 concludes this article.

2 THEORETICAL CONCEPTS

2.1 Classical spin models

A classical spin model is the classical limit of a quantum mechanical, localized spin model – the Heisenberg model (Heisenberg, 1928) (see Steevens, 1963; Anderson, 1963; Levy, 2000, for the theoretical background). The Hamiltonian of a classical spin model describing a magnetic system may contain contributions from exchange interactions, crystalline anisotropies, the external magnetic field, and dipole–dipole interactions. There might also be other contributions (e.g., a magnetovolume coupling) which, for the sake of simplicity, will not be considered in the following. An appropriate Hamiltonian may then be written in the form

$$\mathcal{H} = \mathcal{H}_{\text{exc}} + \mathcal{H}_{\text{anis}} + \mathcal{H}_{\text{field}} + \mathcal{H}_{\text{dipol}} \tag{1}$$

Within the framework of the classical Heisenberg model the exchange energy is expressed as

$$\mathcal{H}_{\text{exc}} = -\sum_{\langle ij \rangle} J_{ij} \mathbf{S}_i \cdot \mathbf{S}_j \tag{2}$$

where the $\mathbf{S}_i = \boldsymbol{\mu}_i / \mu_s$ are three-dimensional magnetic moments reduced to unit length. This part represents the exchange of the magnetic moments and it is often (but not necessarily) restricted two nearest-neighbor interactions with a unique exchange coupling constant J. For $J > 0$ this part of the Hamiltonian leads to ferromagnetic order while for $J < 0$ it can lead to antiferromagnetic order if the lattice structure allows for antiferromagnetic order without frustration effects.

The simplest example for a crystalline anisotropy is

$$\mathcal{H}_{\text{anis}} = -d_z \sum_i S_{iz}^2 \tag{3}$$

which is a uniaxial anisotropy favoring the z axis as easy axis of the system for positive anisotropy constant d_z. Of course, other anisotropy terms describing any crystalline, stress, or surface anisotropies could also be considered.

The Zeeman energy is

$$\mathcal{H}_{\text{field}} = -\mathbf{b} \cdot \sum_i \mathbf{S}_i \tag{4}$$

describing the coupling of the moments to an external magnetic field with $\mathbf{b} = \mu_s \mathbf{B}$. Here, μ_s is the absolute value of the magnetic moment which for an atomic moment is of the order of a Bohr magneton.

The dipole–dipole coupling of the magnetic moments leads to an energy

$$\mathcal{H}_{\text{dipole}} = -w \sum_{i<j} \frac{3(\mathbf{S}_i \cdot \mathbf{e}_{ij})(\mathbf{e}_{ij} \cdot \mathbf{S}_j) - \mathbf{S}_i \cdot \mathbf{S}_j}{r_{ij}^3} \tag{5}$$

with $w = \mu_s^2 \mu_0 / 4\pi a^3$ when the spins are on a regular lattice with spacing a. The atomic magnetic moments are handled in a point dipole approximation. The r_{ij} are the normalized distances between moments i and j and the $\mathbf{e}_{ij}$ are unit vectors in the direction of $\mathbf{r}_{ij}$. Since the dipole–dipole interaction of two moments depends on their distance vector, the dipolar energy contribution will depend on the shape of the sample. Dipoles try to be aligned, minimizing free surface charges, which leads to shape anisotropy and to the fact that domain structures may minimize the energy of the system. Hence, dipole–dipole coupling is the microscopic origin of the magnetostatic stray field energy.

Classical spin models are in some sense 'between' a full quantum mechanical first-principles description and a micromagnetic continuum approach. But they can also be interpreted as the discretized version of a micromagnetic continuum model, where the charge distribution for a single cell of the discretized lattice is approximated by a point dipole (Berkov, Ramstöck and Hubert, 1993; Hubert and Schäfer, 1998). Also, for certain magnetic systems their description in terms of a lattice of magnetic moments is based on the mesoscopic structure of the material, especially when a particulate medium is described (Chantrell, Lyberatos and Wohlfarth, 1986; Nowak, Rüdiger, Fumagalli and Güntherodt, 1996; Nowak, 1997; Nowak, Heimel, Kleinefeld and Weller, 1997; Chantrell, Walmsley, Gore and Maylin, 2000; Verdes *et al.*, 2002). In this case it is assumed that one grain or particle can be described by a single magnetic moment. Therefore, the size of the particles and the temperature must be small enough so that internal degrees of freedom are not relevant for the special problem under consideration.

When compared, the use of classical spin models for the description of magnetic materials has advantages as well as disadvantages. The main disadvantage is that owing to the atomic resolution the system size is clearly restricted to a nanoscale (at the moment to the order of, say, 10^7 spins, steadily increasing with computational power). But the advantages are (i) realistic lattice structures and interactions can be taken into account without assuming a continuous magnetization (Vedmedenko *et al.*, 2004), (ii) finite temperatures can be taken into account without cutting the spin-wave spectra because of the discretization (Berkov, 2007), (iii) the form and the parameters of the Hamiltonian can be derived from first-principles calculations (see e.g., Mryasov, Nowak, Guslienko and Chantrell, 2005), and (iv) the modeling of

para-, ferri-, ferro- or antiferromagnets, and even heterostructures composed of several of these different materials is straightforward.

Hence typical magnetic systems for a description using classical spin models are nanostructures or systems with very narrow domain walls (Garanin, 1991; Kazantseva, Wieser and Nowak, 2005), especially when thermal excitations are relevant (Garanin, 1997; Nowak, 2001), and magnetic heterostructures including antiferromagnetic components (Malozemoff, 1987; Nowak *et al.*, 2002b).

2.2 Thermodynamics and the equation of motion

In order to calculate thermodynamic equilibrium properties one has to calculate thermal averages for the properties of interest. For instance, in a canonical ensemble the temperature-dependent reduced magnetization becomes

$$\mathbf{m}(T) = \frac{1}{N}\left\langle \sum_i \mathbf{S}_i \right\rangle = \frac{1}{N} \mathrm{Tr}\, \frac{1}{Z} e^{-\mathcal{H}/k_\mathrm{B}T} \sum_i \mathbf{S}_i \qquad (6)$$

where $\langle \ldots \rangle$ denotes a thermal average and $Z = \mathrm{Tr}\, e^{-\mathcal{H}/k_\mathrm{B}T}$ is the canonical partition function (see, e.g., Reif, 1965). For N classical spins the calculation of the trace would involve an integral over phase space, that is, integrals over N unit spheres. This high-dimensional integral can usually not be calculated exactly for realistic magnetic systems. Instead either approximations have to be used, the most famous one being the mean-field approximation (Wagner, 1972; Levy, 2000) or numerical techniques like Monte Carlo methods.

Moreover, one often is interested in nonequilibrium properties. Then, the basic equation of motion for magnetic moments coupled to a heat bath is the LLG equation (Landau and Lifshitz, 1935; Gilbert, 1955; Brown, 1963a) with Langevin dynamics. For electronic magnetic moments it can be written in the form

$$\dot{\mathbf{S}}_i = -\frac{\gamma}{(1+\alpha^2)\mu_s} \mathbf{S}_i \times \left(\mathbf{H}_i(t) + \alpha\, \mathbf{S}_i \times \mathbf{H}_i(t) \right) \qquad (7)$$

where $\gamma = 1.76 \times 10^{11}(\mathrm{T\,s})^{-1}$ is the absolute value of the gyromagnetic ratio and $\mathbf{H}_i(t) = \boldsymbol{\zeta}_i(t) - \partial\mathcal{H}/\partial\mathbf{S}_i$. The thermal noise $\boldsymbol{\zeta}_i(t)$ obeys

$$\langle \boldsymbol{\zeta}_i(t) \rangle = 0 \qquad (8)$$

$$\langle \zeta_{i\eta}(t)\zeta_{j\theta}(t') \rangle = \delta_{i,j}\delta_{\eta,\theta}\delta(t-t')2\alpha k_\mathrm{B}T\mu_s/\gamma \qquad (9)$$

i and j denote once again the sites of the lattice and η and θ the Cartesian components. The first part of equation (7) describes the spin precession, which can be derived from Heisenberg's equation of motion in the classical limit, while the second part includes the relaxation of the moments. α is a dimensionless parameter describing phenomenologically the strength of the coupling to the heat bath. Note, that this microscopic coupling parameter is not necessarily identical with the usual macroscopic damping parameter (Chubykalo, Nowak, Chantrell and Garanin, 2006) but we will, nevertheless, refer to α as damping parameter in the following. As a consequence of the fluctuation dissipation theorem, α governs the relaxation aspect of the coupling to the heat bath as well as the fluctuations via the strength of the thermal noise (Lyberatos and Chantrell, 1993; Chubykalo *et al.*, 2003b; Berkov, 2007). The assumption of uncorrelated noise on an atomic level is a simplification reflecting the lack of knowledge regarding the fundamental physical mechanisms involved in the coupling between spins and heat bath. The microscopic understanding of damping is an outstanding challenge for current research (Smith and Arnett, 2001; Safonov and Bertram, 2002; Rebei and Parker, 2003). However, the strength of the noise in equation (9) ensures correct thermal averages.

One can solve the LLG equation easily for an isolated spin coupled to an external field $\mathbf{B}$, neglecting the thermal fluctuations. Then the first term in equation (7) leads to a spin precession with the precession time $\tau_p = 2\pi(1+\alpha^2)/(\gamma B)$. The second part describes a relaxation of the spin from an initial state into local equilibrium on the relaxation timescale $\tau_r = \tau_p/\alpha$. In other words, α sets the relation between the timescales of precession and relaxation. In the high damping limit, which in the following will turn out to be important in connection with Monte Carlo simulations, mainly the second term of the LLG equation is relevant and the time can be rescaled by the factor $(1+\alpha^2)\mu_s/(\alpha\gamma)$. Hence, this factor should completely describe the α and γ dependence of any timescale in the high damping limit.

The LLG equation is a stochastic equation of motion. Starting repeatedly from identical initial conditions will lead to different trajectories in phase space because of the influence of noise. Hence, averages have to be taken in order to describe the system appropriately. The basis for the statistical description of an ensemble of systems where each one is described by a Langevin equation is the corresponding Fokker–Planck (FP) equation. This is a differential equation for the time evolution of the probability distribution in phase space (Coffey, 1996). In his pioneering work Brown (1963b) developed a formalism for the description of thermally activated magnetization reversal on the basis of the FP equation which led to a low-temperature asymptotic formula for the escape rates in simple magnetic systems (for an overview see Coffey, 1996). The solution of the FP equation will converge to equilibrium properties, that is to the same values defined by equation (6).

However, realistic calculations for systems with many degrees of freedom need computational approaches. The two basic methods for the simulation of classical spin systems are Langevin dynamics and Monte Carlo methods. The following section is devoted to these methods, especially to their relation which will lead to time-quantified Monte Carlo methods.

3 NUMERICAL METHODS

3.1 Langevin dynamics simulations

The basic numerical approach for the description of thermally activated spin dynamics is the direct numerical integration of equation (7). Instead of solving the corresponding FP equation, one calculates trajectories in phase space following the underlying equation of motion. In order to obtain results in the sense of a thermodynamic average one has to calculate many of these trajectories starting with the same initial conditions, taking an average over these trajectories for the quantities of interest. This method is referred to as *Langevin dynamics simulation* (Lyberatos and Chantrell, 1993).

The LLG equation with Langevin dynamics is a stochastic differential equation with multiplicative noise. For this kind of differential equation a problem arises which is called the *Itô–Stratonovich dilemma* (Greiner, Strittmatter and Honerkamp, 1988). As a consequence, different time discretization schemes may with decreasing time step converge to different results (see Wolf, 1998, for a discussion of the different discretization schemes from a physical point of view). As was pointed out by García-Palacios and Lázaro (1998) the multiplicative noise in the Langevin equation was treated in Brown's original work – and also in subsequent publications – by means of the Stratonovich interpretation. Hence, in order to obtain numerical results that are comparable to these approaches via the FP equation one has to use adequate methods. Note, that the simplest method for the integration of first-order differential equations, the Euler method, converges to an Itô interpretation of the Langevin equation. The simplest appropriate discretization scheme leading to a Stratonovich interpretation is the Heun method (Greiner, Strittmatter and Honerkamp, 1988; Wolf, 1998; García-Palacios and Lázaro, 1998; Nowak, 2001) which is described in the following [1].

For simplicity, the Heun discretization scheme is introduced here for a one-dimensional problem. We consider a first-order differential equation with multiplicative noise,

$$\dot{x}(t) = f\Big(x(t), t\Big) + g\Big(x(t), t\Big)\zeta(t) \tag{10}$$

where $\zeta(t)$ represents a noise with a distribution of moments $\langle\zeta(t)\rangle = 0$ and $\langle\zeta(t)\zeta(t')\rangle = D\delta(t-t')$. The time variable is discretized in intervals Δt so that $t_n = n\Delta t$ and $x_n = x(t_n)$. Then, owing to Heun's method equation (7) becomes

$$\begin{aligned} x_{n+1} = x_n &+ \frac{1}{2}\Big(f(x_n, t_n) + f(\overline{x}_{n+1}, t_{n+1})\Big)\Delta t \\ &+ \frac{1}{2}\Big(g(x_n, t_n) + g(\overline{x}_{n+1}, t_{n+1})\Big)\tilde{\zeta}_n \end{aligned} \tag{11}$$

This method is a predictor–corrector method where the predictor $\overline{x}_{n+1}$ is calculated from an Euler integration scheme,

$$\overline{x}_{n+1} = x_n + f(x_n, t_n)\Delta t + g(x_n, t_n)\tilde{\zeta}_n$$

$\tilde{\zeta}_n$ are random numbers with a distribution characterized by the two first moments $\langle\tilde{\zeta}_n\rangle = 0$ and $\langle\tilde{\zeta}_n\tilde{\zeta}_m\rangle = D\Delta t\delta_{n,m}$, which can be achieved by use of random numbers with a Gaussian distribution, $p(\zeta) \sim \exp(-\zeta^2/2\sigma)$, with width $\sigma = D\Delta t$. The generalization of the scheme in the preceding text to equation (7) is straightforward.

3.2 Monte Carlo methods

Monte Carlo methods are well established in the context of equilibrium thermodynamics, where mainly Ising-type models have been investigated because of the broad variety of applications of this class of models in statistical physics (Stauffer, Hehl, Winkelmann and Zabolitzky, 1993; Binder and Heermann, 1997). However, in the context of magnetic materials the use of Ising models is restricted to the modeling of materials with a very large uniaxial anisotropy (Kirby, Shen, Hardy and Sellmyer, 1994; Lyberatos, Earl and Chantrell, 1996; Nowak, Heimel, Kleinefeld and Weller, 1997), while more realistic models have to include finite anisotropies.

Within a Monte Carlo approach trajectories in phase space are calculated following a master equation (Reif, 1965) for the time development of the probability distribution $P_s(t)$ in phase space,

$$\frac{\mathrm{d}P_s}{\mathrm{d}t} = \sum_{s'}\left(P_{s'}w_{s'\to s} - P_s w_{s\to s'}\right) \tag{12}$$

Here, s and s' denote different states of the system and the w are the transition rates from one state to another one which have to fulfill the condition (Reif, 1965)

$$\frac{w_{s\to s'}}{w_{s'\to s}} = \exp\left(\frac{E(S) - E(S')}{k_\mathrm{B}T}\right) \tag{13}$$

The master equation describes exclusively the coupling of the system to the heat bath. Hence, only the irreversible part of the dynamics of the system is considered including the relaxation and the fluctuations, but not the energy conserving part of the equation of motion – the precession. Instead, only a random-walk-like motion due to the coupling to the heat bath can appear. We will discuss the connection to Langevin dynamics later and continue with a general description of Monte Carlo algorithms for vector spin models, as far as they are different from algorithms for Ising models due to their continuum degrees of freedom.

Even though for Ising systems (Swendsen and Wang, 1987) as well as for Heisenberg systems (Wolff, 1989) cluster algorithms exist, which – depending on the details of the problem – can equilibrate a system much faster, we restrict ourselves to the simple case of single-spin-flip dynamics since here, the connection to a realistic dynamical behavior of the system is more straightforward. For the Ising model there exists no equation of motion and the master equation in connection with a single-spin-flip dynamics governs the so-called Glauber dynamics (Glauber, 1963), which is thought to describe a qualitatively realistic dynamic behavior. For a system of classical magnetic moments the situation is different due to the existence of an equation of motion – the LLG equation.

A single-spin-flip algorithm is performed in the following way: at the beginning one single spin from the lattice is chosen either randomly or in some systematic order and a trial step of this selected spin is made (possible choices for trial steps will be described in detail in the subsequent text). Then the change of the energy of the system is computed according to equation (1). Finally the trial step is accepted, for instance with the heat bath probability,

$$w_{s\to s'} = \frac{w_0}{1+\exp\left(\frac{E(S')-E(S)}{k_B T}\right)} \tag{14}$$

which is one possible choice among others satisfying the condition in equation (13) for any arbitrary constant w_0. Scanning the lattice and performing the procedure explained in the preceding text once per spin (on average) is called *one Monte Carlo step* (MCS). It defines a quasitime scale of the simulation. The connection to real time will be discussed later on.

The way the trial step is chosen is of importance for the validity and efficiency of the algorithm as well as for the physical interpretation of the dynamic behavior of the algorithm (Hinzke and Nowak, 1999). For an Ising system the trial step is naturally a spin flip. For a Heisenberg spin there are many choices. One possible trial step is a small deviation from the former state. For a spin this could be a random movement of the spin with uniform probability distribution within a given opening angle around the former spin direction. Here, each spin can only move by a limited step size and hence, in a model with a uniaxial anisotropy, it has to overcome the anisotropy energy barrier for a complete reversal. This might be a realistic choice for many model systems. But if one is, for instance, interested in the crossover from Heisenberg to Ising-like behavior with increasing anisotropy, one has to allow also for larger steps which are able to overcome a given anisotropy energy barrier. Otherwise the dynamics of the system would freeze and in a system with very large anisotropy (Ising limit) no spin flip would occur at all (Hinzke and Nowak, 1999).

Another possible trial step that circumvents this problem is a step with a uniform distribution in the entire phase space. Here, an arbitrary spin direction that does not depend on the initial direction of the spin is chosen at random. This step samples the whole phase space efficiently and a single spin is not forced to overcome the anisotropy energy barrier. Instead it is allowed to change from one direction to any other one instantaneously. Both of these trail steps are allowed choices in the sense that the corresponding algorithms lead to correct equilibrium properties since they fulfill two necessary conditions: they are ergodic and symmetric.

Ergodicity requires that the whole phase space can be sampled by an algorithm. An example for an nonergodic algorithm is one that performs only Ising-like trial steps, $S_z \to -S_z$, in a Heisenberg model. Here, starting from some initial direction the spin can only reach two positions out of the whole phase space which would be a unit sphere for a Heisenberg spin. Nevertheless, one is allowed to perform such reflection steps as long as one uses *also* other trial steps that guarantee ergodicity. These ideas lead to combinational algorithms which – depending on the problem – can be very efficient (Hucht, Moschel and Usadel, 1995; Hinzke and Nowak, 1999).

The second condition that has to be fulfilled by any algorithm is a symmetry condition: for the probability to do a certain trial step it must be $p_t(s \to s') = p_t(s' \to s)$. Otherwise equation (13) is not fulfilled since the probabilities to perform certain trial steps contribute to the transition rates. The symmetry condition would for instance be violated in a Heisenberg system if one chooses new trial spin directions by simply generating three random numbers as S_x, S_y, and S_z coordinates within a cube and normalizing the resultant vector to unit length. Then before normalization the random vectors are homogeneously distributed within the cube and after the normalization they have some nonuniform probability distribution on the unit sphere which is higher along the diagonal directions of the cube. Hence, trial steps from any other direction into the diagonal direction are more probable then vice versa and the algorithm yields wrong results. A description, how to choose unit vectors

with random directions and a constant probability distribution correctly can be found in the book of Vesely (1993).

3.3 Time-quantified Monte Carlo simulations

In general, Monte Carlo methods do not allow for an interpretation of the results in terms of a realistic dynamics. Only recently, a time-quantified Monte Carlo method was introduced (Nowak, Chantrell and Kennedy, 2000; Smirnov-Rueda *et al.*, 2000; Chubykalo *et al.*, 2003a; Cheng, Jalil, Lee and Okabe, 2006) and it was shown that at least the dynamics of a high damping scenario can indeed be simulated by a Monte Carlo simulation since here the exact knowledge of the precessive motion of the spins is not necessary. The main idea of time-quantified Monte Carlo methods is to compare the fluctuations that are established in the Monte Carlo simulation within one MCS with the fluctuations that are established within a given timescale associated with the linearized stochastic LLG equation (Ettelaie and Moore, 1984; Smirnov-Rueda *et al.*, 1999).

Following the original work (Nowak, Chantrell and Kennedy, 2000), we start with a calculation of the magnetization fluctuations in the Langevin equation. Close to a local energy minimum one can expand the energy of a system given that first-order terms vanish as

$$E \approx E_0 + \frac{1}{2}\sum_{i,j} A_{ij} S_i S_j \tag{15}$$

where S_i are now variables representing small deviations from equilibrium. Let us consider a single spin only with a uniaxial anisotropy (anisotropy constant d_z, see equation (3)) and a field $\mathbf{b} = \pm b_z \hat{\mathbf{z}}$, which is also aligned with the easy axis (a more general calculation can be found in Chubykalo *et al.*, 2003b). In this system, we find equilibrium along the z axis, leading to variables S_x and S_y describing small deviations from the equilibrium position $\mathbf{S} = \pm\hat{\mathbf{z}}$. The energy increase ΔE associated with fluctuation in S_x and S_y is then simply

$$\Delta E \approx \frac{1}{2}\left(A_{xx} S_x^2 + A_{yy} S_y^2\right) \tag{16}$$

with $A_{xx} = A_{yy} = 2d_z + b_z$. Rewriting the LLG equation in the linearized form without the thermal fluctuations,

$$\begin{aligned} \dot{S}_x &= L_{xx} S_x + L_{xy} S_y \\ \dot{S}_y &= L_{yx} S_x + L_{yy} S_y \end{aligned} \tag{17}$$

we can identify the matrix elements

$$\begin{aligned} L_{xx} = L_{yy} &= -\frac{\alpha\gamma}{(1+\alpha^2)\mu_s}(2d_z + b_z) \\ L_{xy} = -L_{yx} &= \frac{\gamma}{(1+\alpha^2)\mu_s}(2d_z + b_z) \end{aligned}$$

As shown in Lyberatos, Berkov and Chantrell (1993) the correlation function for the variables describing small deviations from equilibrium can be expressed in the form

$$\langle S_i(t) S_j(t') \rangle = \mu_{ij} \delta_{ij} \delta(t - t') \tag{18}$$

Here, i and j denote the Cartesian components and Dirac's δ function is an approximation for exponentially decaying correlations on timescales $t - t'$ that are larger than the timescale of the exponential decay τ_r. The covariance matrix μ_{ij} can be calculated from the system matrices A_{ij} and L_{ij} as (Lyberatos, Berkov and Chantrell, 1993)

$$\mu_{ij} = -k_B T \left(L_{ik} A_{kj}^{-1} + L_{jk} A_{ki}^{-1}\right)$$

For our problem this yields

$$\begin{aligned} \mu_{xx} = \mu_{yy} &= 2k_B T \frac{\alpha\gamma}{(1+\alpha^2)\mu_s} \\ \mu_{xy} = \mu_{yx} &= 0 \end{aligned} \tag{19}$$

Integrating the fluctuating quantities $S_x(t)$ and $S_y(t)$ over a finite time interval Δt, equations (18) and (19) yield

$$\langle \bar{S}_x^2 \rangle = \langle \bar{S}_y^2 \rangle = 2k_B T \frac{\alpha\gamma}{(1+\alpha^2)\mu_s} \Delta t \tag{20}$$

representing the fluctuations of $S_x(t)$ and $S_y(t)$ respectively, averaged over a time interval Δt.

For comparison, we now calculate the fluctuations $\langle S_x^2 \rangle$ which are established within one MCS of a Monte Carlo simulation (Nowak, Chantrell and Kennedy, 2000). We select an algorithm where the trial step of the Monte Carlo algorithm is a random deviation of the magnetic moment from its former direction up to a certain maximum opening angle. In order to achieve this efficiently one first constructs a random vector with constant probability distribution within a sphere of radius R by use of the rejection method (Vesely, 1993). This random vector is then added to the initial moment and subsequently the resulting vector is again normalized. Note that the probability distribution following from this trial step is nonuniform but isotropic, so that the symmetry condition mentioned in the previous subsection is guaranteed.

For this algorithm the probability distribution for trial steps of size $r = \sqrt{S_x^2 + S_y^2}$ is $p_t = 3\sqrt{R^2 - r^2}/(2\pi R^3)$ for $0 < r < R$. The acceptance probability using a heat bath

algorithm is $w(r) = 1/(1 + \exp(\Delta E(r^2)/k_B T))$. Assuming that the spin is close to its (local) equilibrium position, as before, $\Delta E(r^2)$ for small r can be taken from equation (16). In order to calculate the fluctuations within one MCS we have to integrate over that part of the phase space that can be reached within one MCS,

$$\langle S_x^2 \rangle = \int_0^{2\pi} \mathrm{d}\varphi \int_0^R r\,\mathrm{d}r\,\frac{r^2}{2}\,w(r)p_t(r) = \frac{R^2}{10} - \mathcal{O}\left(\frac{(2d_z + b_z)R^4}{k_B T}\right) \tag{21}$$

where the last line is an expansion for small R leading to the validity condition

$$R \ll \frac{k_B T}{(2d_z + b_z)} \tag{22}$$

By equalizing the fluctuations within a time interval Δt of the LLG equation and one MCS we find the relation

$$R^2 = \frac{20 k_B T \alpha \gamma}{(1 + \alpha^2)\mu_s}\Delta t \tag{23}$$

for the trial step width R (Nowak, Chantrell and Kennedy, 2000). Equation (23) now relates one MCS, performed using an algorithm as explained before, with a real time interval of the Langevin equation. In this equation $(\alpha\gamma/(1 + \alpha^2)\mu_s)\Delta t$ is simply the reduced time of the LLG equation, rescaled in the high damping limit where only the second part of equation (7) is relevant. The more interesting result of equation (23) is the temperature dependence since it turns out that there is no trivial assignment of one MCS to a fixed time interval. Instead, the larger the temperature, the larger the trial steps of the Monte Carlo algorithm in order to allow for the appropriate fluctuations.

In principle, equation (23) gives the possibility to choose the trial step width for a Monte Carlo simulation in such a way that one MCS corresponds to some microscopic time interval, but there are of course restrictions for possible values of the trial step width and also for the validity of the algorithm: R must be small enough so that the truncated expansion in equation (21) is a good approximation. On the other hand R should not be too small since otherwise the Monte Carlo algorithm needs too much computation time to sample the phase space. Therefore, either one chooses such a value for Δt so that R takes on reasonable values or one chooses a reasonable constant value for R and uses equation (23) to calculate Δt as the real time interval associated with one MCS. Furthermore, effects from spin precession are neglected so that in general only the high damping limit with a purely diffusive spin motion can be simulated. Also, since the derivation in the preceding text started from a linearized equation of motion (equation (17)) and since the energy expression (equation (15)) is an expansion, equation (23) can only be valid close to equilibrium.

For any numerical method, analytically solvable models are important as test tools for the evaluation of the numerical techniques. Originally, (Nowak, Chantrell and Kennedy, 2000) the goal was a comparison of characteristic timescales for the thermally activated reversal obtained numerically with those following from an analytical treatment of isolated Stoner–Wohlfarth particles with a uniaxial anisotropy and a field at an oblique angle to the easy axis (Coffey *et al.*, 1998c). The results are shown in Figure 1.

Here, an ensemble of isolated single-domain particles is considered where each particle is represented by a magnetic moment with energy

$$E(\mathbf{S}) = -d_z S_z^2 - \mu_s \mathbf{B}\cdot\mathbf{S} \tag{24}$$

The material parameters are those for a 20-nm Co particle. Both of the simulations, Monte Carlo as well as Langevin dynamics, start with the magnetic moments in positive z direction. The magnetic field which is well below the Stoner–Wohlfarth limit for athermal reversal has a negative z component so that the magnetization will reverse after some time. The time that is needed for the z component of the magnetization to change its sign averaged over a large number of runs ($N = 1000$) is the numerically obtained characteristic time τ. During a simulation for temperatures which are low as compared to the energy barrier, the system is in the metastable, initial state for a very long time, while the time needed for the magnetization reversal itself is

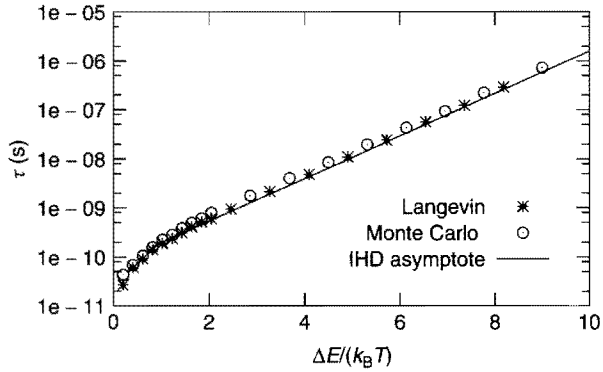

Figure 1. Characteristic times versus inverse temperature. Comparison of the intermediate to high damping asymptote with results from Langevin dynamics and Monte Carlo simulations with time quantification. (Reprinted figure with permission from *Physical Review Letters*, **84**, 1, 163, 2000. Copyright 2000 by the American Physical Society.)

rather short. In this case the characteristic time τ should be comparable to the escape time following from an analytical calculation via the FP equation.

The time-quantified Monte Carlo simulations in Figure 1 were done with an algorithm using a trial step according to equation (23) with $\Delta t \approx 6 \times 10^{-12}$ s and $\alpha = 1$. The magnetic field is $|\mathbf{B}| = 0.2$ T with an angle of 27° to the easy axis. The results for $\tau(T)$ are compared with results from Langevin dynamics simulations using the Heun method as described before and with analytical results obtained in the intermediate to high damping (IHD) limit (Coffey *et al.*, 1998a,b,c). This asymptote has the general form of a thermal activation law, namely

$$\tau = \tau_0 e^{\Delta E / k_B T} \tag{25}$$

The explicit expressions for τ_0 and ΔE were derived in Coffey *et al.* (1998a,b,c). The validity condition for the IHD formula is $\alpha \Delta E / k_B T \gg 1$ which has been satisfied in the case presented here.

From Figure 1 it is clear that the Langevin dynamics data agree very well with the analytical asymptote in the preceding text. For higher temperatures, $k_B T > \Delta E$, the asymptote is no longer appropriate. Here, the numerical data for τ tend to zero for $T \to \infty$ as one expects. The Monte Carlo data deviate slightly but the agreement is remarkable – especially taking into account the simple form of equation (23) underlying this algorithm and also considering the fact that there is no adjustable parameter in all our simulations and formulae.

Figure 2 shows how the time-quantified Monte Carlo methods converges in the high damping limit. The data were obtained for the same parameter values as before and $\Delta E / k_B T = 3.3$. The figure shows that for increasing damping constant α the Monte Carlo data converge to the IHD formula and to the data from Langevin dynamics simulation for large α.

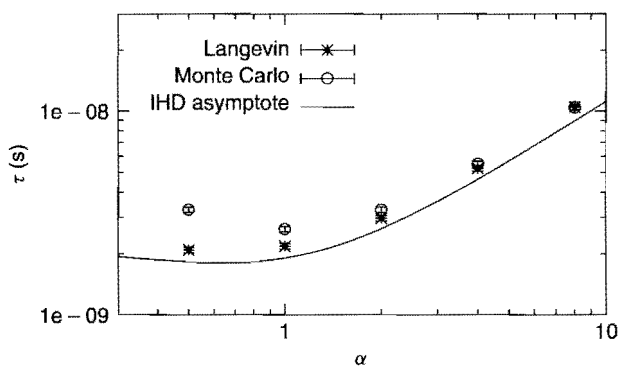

Figure 2. Characteristic time versus damping constant: comparison of the intermediate to high damping asymptote with Langevin dynamics and Monte Carlo simulations. (Reprinted figure with permission from *Physical Review Letters*, **84**, 1, 163, 2000. Copyright 2000 by the American Physical Society.)

Even though the Monte Carlo time step quantification by equation (23) was derived originally only for the simple system which we considered here (Nowak, Chantrell and Kennedy, 2000), it turned out to be successfully applicable to more complicated, interacting spin systems also (Hinzke and Nowak, 2000a,b; Chubykalo *et al.*, 2003a,b; Cheng, Jalil, Lee and Okabe, 2006). However, one should note that the method rests on a comparison with Langevin dynamics. Here, the coupling to the heat bath is added phenomenologically to the equation of motion leading to a damping constant α, the microscopic evaluation of which is still missing.

4 THERMALLY ACTIVATED MAGNETIZATION REVERSAL

4.1 Introduction

The understanding of thermally activated spin dynamics is a major challenge for the knowledge of magnetic systems and devices. The pioneering work of Brown (1963b) represents the basis for the understanding of thermally activated dynamic processes in isolated single-domain particles. The basic idea is that the energy barrier ΔE separating two (meta)stable magnetic states of a nanoparticle can be overcome by thermal activation on a certain timescale which can be calculated within the framework of Langevin dynamics. In the limit of low temperatures the escape time τ follows a thermal activation law (see equation (25)), where the prefactor as well as the energy barrier depend on the mechanism of the reversal. As a solvable example, Brown considered an ensemble of isolated magnetic moments with a uniaxial anisotropy. Each single particle of the ensemble is described as one superspin of constant length. The superspin is thought to represent the magnetic moment of a whole particle since it was assumed that if the particle is sufficiently small it is always homogeneously magnetized and its microscopic, internal degrees of freedom can be neglected. After the original work of Brown, extensive calculations were performed in order to calculate the energy barrier as well as the prefactor asymptotically for various model systems (Aharoni, 1969; Braun, 1993; Coffey *et al.*, 1998a; García-Palacios and Svedlindh, 2000; Chantrell, Walmsley, Gore and Maylin, 2000).

Experiments on isolated, magnetic particles have confirmed this approach. Wernsdorfer *et al.* measured the switching time of isolated nanometer-sized particles (Wernsdorfer

et al., 1996b, 1997b), and wires (Wernsdorfer *et al.*, 1996a, 1997a). For sufficiently small particles (Wernsdorfer *et al.*, 1997b) agreement was found with the theoretical predictions of Brown (1963b). For larger particles (Wernsdorfer *et al.*, 1996b) and wires (Wernsdorfer *et al.*, 1996a, 1997a) activation volumes were found which were much smaller than the corresponding particle and wire volumes. Obviously, different reversal mechanisms can dominate the thermally activated switching behavior of nanoparticles depending on their geometry and size, such as coherent rotation, nucleation, and curling.

These modes may appear in different limits of a cylindrical geometry. Coherent rotation and nucleation can be modeled in the one-dimensional limit by a simple spin chain – a model which is very useful since it was treated analytically and asymptotic results for the energy barriers as well as for the escape rates are available (Braun, 1993; 1994a,b). We will discuss this model in the following text. A three-dimensional model for an extended nanowire is discussed in the last subsection in connection with curling.

Let us start with a chain of magnetic moments of length L (number of spins) with periodical boundary conditions defined by the Hamiltonian

$$\mathcal{H} = \sum_i \left[-J\mathbf{S}_i \cdot \mathbf{S}_{i+1} - d_z (S_i^z)^2 + d_x (S_i^x)^2 - \mu_s B S_i^z \right] \tag{26}$$

This is a discretized version of the one-dimensional model for a magnetic nanowire considered by Braun (1993). For $d_z, d_x > 0$ the z axis is the easy axis and the x axis the hard axis of the system. These anisotropy terms may contain contributions from shape anisotropy as well as crystalline anisotropies (Braun, 1994a). In the interpretation as shape anisotropy, this single-ion anisotropy is assumed to imitate the influence of a dipolar interaction of strength $w = d_z/\pi$ (Braun, 1993). Nevertheless, an exact numerical treatment of the dipolar interactions is possible (Hinzke and Nowak, 2000b; Nowak, 2001; Nowak *et al.*, 2005; Wieser, Usadel and Nowak, 2006).

4.2 Coherent rotation

In the case of small chain length the magnetic moments rotate coherently, minimizing the exchange energy while overcoming the energy barrier due to the anisotropy of the system. Owing to the hard-axis anisotropy the rotation is mainly in the yz plane. As long as all spins are mostly parallel, they can be described as one effective magnetic moment which behaves like the one-spin model described before. The corresponding energy barrier ΔE is the same as that of a Stoner–Wohlfarth particle since the additional hard axis does not change the energy of the optimal path in phase space from one minimum to the other. The escape time was calculated from the FP equation in the large damping limit (Braun, 1994b). The results is a thermal activation law (equation (25)) where the energy barrier is now proportional to the system size L,

$$\Delta E_{\mathrm{cr}} = L d_z (1-h)^2 \tag{27}$$

while the explicit form of the prefactor transformed into the units used here is

$$\tau_{\mathrm{cr}} = \frac{2\pi(1+\alpha^2)}{\alpha\gamma B_{\mathrm{c}}} \times \frac{\sqrt{d(1+h)/(1-h+d)}}{1-h^2-d+\sqrt{(1-h^2+d)^2+4d(1-h^2)/\alpha^2}} \tag{28}$$

We introduced the coercive field $B_{\mathrm{c}} = 2d_z/\mu_s$ and the reduced quantities $h = \mu_s B/(2d_z)$ and $d = d_x/d_z$. The first term in equation (28) is the microscopic relaxation time of one spin in the field B_{c} (see Section 2.1), while the second term includes corrections following from the details of the model. The equation in the preceding text should hold for low temperatures $k_{\mathrm{B}}T \ll \Delta E_{\mathrm{cr}}$ and obviously for $B < B_{\mathrm{c}}$ since otherwise the energy barrier is zero, leading to a spontaneous reversal without thermal activation. Note, however, that recently deviations were found for increasing system size, suggesting that even for a coherent rotation the internal degrees of freedom lead to longitudinal fluctuations which are not contained in a single-spin description (Hinzke and Nowak, 2000a; Nowak *et al.*, 2005; Chubykalo, Nowak, Chantrell and Garanin, 2006).

4.3 Soliton–antisoliton nucleation

With increasing system size nucleation must become energetically favorable since here the energy barrier is a constant, while it is proportional to the system size in the case of coherent rotation. For the spin chain under consideration, switching by soliton–antisoliton nucleation was proposed (Braun, 1994a) for sufficiently large system size. Here, the nucleation process initiates a pair of domain walls which splits the system into domains with opposite directions of magnetization parallel to the easy axis (for graphical representations see Hinzke, Nowak and Usadel, 2000; Nowak, 2001). These two domain walls pass the system in the subsequent reversal process. Owing to the hard-axis anisotropy the spin rotation is once again mainly in the yz plane. Since these two domain walls necessarily have opposite helicities within this easy plane they were called a *soliton–antisoliton pair*.

The energy barrier $\Delta E_{\rm nu}$ which has to be overcome during this nucleation process is

$$\Delta E_{\rm nu} = 4\sqrt{2Jd_z}\left(\tanh R - hR\right) \tag{29}$$

with $R = \operatorname{arccosh}(\sqrt{1/h})$ (Braun, 1994a). For vanishing magnetic field this energy barrier has the form $\Delta E_{\rm nu}(h = 0) = 4\sqrt{2Jd_z}$ which represents the well-known energy of two Bloch walls (Hubert and Schäfer, 1998). As usual, the corresponding escape time obeys a thermal activation law, where the prefactor has been calculated for various limits (Braun, 1994a). The prefactor obtained in the overdamped limit (equation (5.4) in Braun, 1994a) in our units is

$$\tau_{\rm nu} = \frac{2\pi(1+\alpha^2)}{\alpha\gamma B_{\rm c}} \frac{(\pi k_{\rm B}T)^{1/2}(2J)^{1/4}}{16L\, d_z^{3/4}|E_0(R)|\tanh R^{3/2}\sinh R} \tag{30}$$

As in equation (28) the left part is the microscopic relaxation time of a spin in the coercive field $B_{\rm c}$. The eigenvalue $E_0(R)$ has been calculated numerically (Braun, 1994a). In the limit $h \to 1$ it is $|E_0(R)| \approx 3R^2$. The $1/L$ dependence of the prefactor reflects the size dependence of the probability of nucleation. The larger the system the more probable is the nucleation process and the smaller is the timescale of the relaxation. Furthermore, the prefactor has a remarkable $\sqrt{k_{\rm B}T}$ dependence.

We should note that all the results in the preceding text are for systems with periodic boundary conditions (or rings), which restricts the applicability to finite nanowires where nucleation processes may start at the ends of the sample. Therefore, the case of open boundaries was also considered, analytically (Braun, 1999, 2000) as well as numerically (Hinzke and Nowak, 2000b). Even though the prefactor of the thermal activation law could not be obtained up to now, it was shown (Braun, 1999) that the energy barrier is just halved in that case, due to the fact that in systems with open boundaries the nucleation can set in at only one end. Hence, solitons and antisolitons do not necessarily emerge pairwise. In the case of two solitons (or two antisolitons) nucleating simultaneously at both ends, these cannot annihilate easily in the later stage of the reversal process due to their identical helicity. Instead a 360° domain wall remains in the system.

Let us now investigate the intermediate temperature range. Owing to the larger thermal fluctuations as compared to the sole soliton–antisoliton nucleation several nuclei may grow simultaneously, also depending on system size. Obviously, depending on the nucleation probability many nuclei may arise during the time period of the reversal process (for graphical representations see again Hinzke, Nowak and Usadel, 2000; Nowak, 2001). This multiple nucleation process was investigated mainly in the context of Ising models where it is called *multidroplet nucleation* (a review is given by Rikvold and Gorman, 1994).

The characteristic time $\tau_{\rm mn}$ for the multidroplet nucleation can be estimated with respect to the escape time for a single nucleation process with the aid of the classical nucleation theory (Becker and Döring, 1935). Here, the following scenario is assumed: in the first stage many nuclei of critical size arise within the same time interval. Later these nuclei expand with a certain domain wall velocity v and join each other. This leads to a change of magnetization

$$\Delta M(t) = \int_0^t \frac{(2vt')^D}{\tau_{\rm nu}}\,{\rm d}t' \tag{31}$$

after a time t in D dimensions. The characteristic time when half of the system ($L^D/2$) is reversed is then given by (Rikvold and Gorman, 1994; Hinzke and Nowak, 2000a)

$$\tau_{\rm mn} = \left(\frac{L}{2v}\right)^{\frac{D}{D+1}} \left((D+1)\tau_{\rm nu}^*\right)^{\frac{1}{D+1}} \exp\frac{\Delta E_{\rm nu}}{(D+1)k_{\rm B}T} \tag{32}$$

The domain-wall velocity in a spin chain following the LLG equation for small fields is (Wieser, Nowak and Usadel, 2004)

$$v = \frac{\gamma B}{\alpha} \tag{33}$$

Hence for the one-dimensional system under consideration the characteristic time is given by

$$\tau_{\rm mn} = \sqrt{\frac{\alpha L \tau_{\rm nu}}{\gamma B}} \exp\frac{\Delta E_{\rm nu}}{2k_{\rm B}T} \tag{34}$$

This means that the (effective) energy barrier for the multidroplet nucleation is reduced by a factor 1/2, and the characteristic time no longer depends on the system size since $\tau_{\rm nu}^*$ for the soliton–antisoliton nucleation has a $1/L$ dependence (see equation (30)).

All the different reversal mechanisms mentioned in the previous sections can occur within the same model system – the spin chain – depending on the system size among other parameters. The crossover from coherent rotation to soliton–antisoliton nucleation was studied in Braun (2000) for a periodic system. Here, the value $L_{\rm c}$ of the chain length below which only uniform solutions of the Euler–Lagrange equations of the problem exist (coherent rotation) was calculated to be

$$L_{\rm c} = \pi\sqrt{\frac{2J}{d_z(1-h^2)}} \tag{35}$$

For vanishing magnetic field this crossover length scale is $L_c = \pi\sqrt{2J/d_z}$, a value that is clearly related to the Bloch wall width $\delta = \sqrt{J/2d}$ (Hubert and Schäfer, 1998), because of the fact that two domains walls have to fit into the system during the nucleation process. For a chain with open boundary conditions the crossover length scale is halved since here only one domain wall has to fit into the system (Braun, 2000). One can understand this result from a slightly different point of view also, namely by comparing the energy barrier of soliton–antisoliton nucleation (equation (29)) with that of coherent rotation (equation (27)). This results in a very similar condition for the crossover from coherent rotation to nucleation (Hinzke and Nowak, 2000a), which can also be generalized to higher dimensions (Hinzke and Nowak, 1998).

For even larger system size, multiple nucleation becomes probable. Comparing the escape time for soliton–antisoliton nucleation with the characteristic time for multiple nucleation, one gets for the intersection of these two times the crossover condition (Hinzke and Nowak, 2000a)

$$L_{\mathrm{sm}} = \sqrt{\frac{\gamma B \tau_{\mathrm{nu}} L_{\mathrm{sm}}}{\alpha}} \exp \frac{\Delta E_{\mathrm{nu}}}{2k_{\mathrm{B}}T} \tag{36}$$

The corresponding time L_{sm}/v is the time that a domain wall needs to cross the system. In other words, as long as the time needed for the nucleation event itself is large as compared to the time needed for the subsequent reversal by domain-wall motion, one single nucleus determines the characteristic time. In the opposite case many nuclei will appear during the time needed for the first soliton–antisoliton pair to cross the system, resulting in multidroplet nucleation. These considerations are comparable to calculations in Ising models (Rikvold, Tomita, Miyashita and Sides, 1994).

Figure 3 summarizes the system size dependence of the reduced characteristic time (Hinzke and Nowak, 2000a). Results from Monte Carlo simulations are shown as well as the appropriate asymptotes described in the preceding text for two different temperatures. For small system sizes the spins rotate coherently. Here the energy barrier (equation (27)) is proportional to the system size leading to an exponential increase of τ with system size. Following equation (28) the prefactor of the thermal activation law should not depend on L but, as already mentioned in the preceding text, numerically one finds slight deviations from the asymptotic expressions due to longitudinal magnetization fluctuations (Nowak *et al.*, 2005; Chubykalo, Nowak, Chantrell and Garanin, 2006). In the region of soliton–antisoliton nucleation the energy barrier does not depend on the system size but the prefactor varies as $1/L$ (see equations (29) and (30)). Interestingly, this leads to a decrease of the characteristic time with increasing system size. Therefore, there

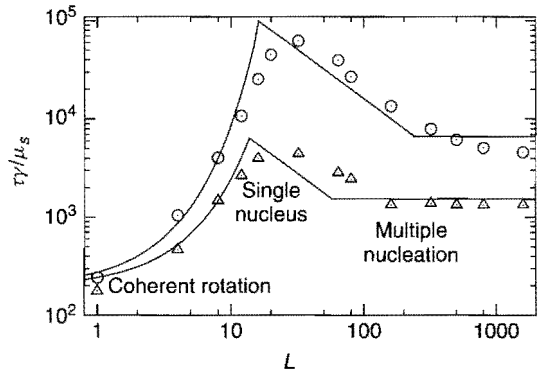

Figure 3. Reduced characteristic time versus system size for $k_{\mathrm{B}}T = 0.024J$ (triangles) and $k_{\mathrm{B}}T = 0.016J$ (circles). $h = 0.75$. Solid lines are piecewise the appropriate asymptotes and the data are from Monte Carlo simulations. (Reprinted from *Phys. Rev. B.*, Vol. 61, 6734, 2000. Copyright 2000 by the American Physical Society.)

is a maximal characteristic time – the maximum of the stability of the particle – close to that system size where the crossover from coherent rotation to nucleation occurs. This decrease ends where multidroplet nucleation sets in, following equation (36). For still larger systems the characteristic time has a constant value which is given by equation (34). Qualitatively the same behavior can be found in the particle size dependence of the dynamic coercivity which is the coercive field one observes during hysteresis on a given timescale τ: solving the equation describing the thermal activation in the three regimes explained in the preceding text for $h(L)$ at constant τ one finds an increase of the dynamic coercivity in the coherent rotation regime, a decrease in the nucleation regime, and at the end a constant value for multiple nucleation. These findings are qualitatively in agreement with measurements of the size dependence for the dynamic coercivity of barium ferrite recording particles (Chang, Zhu and Judy, 1993).

4.4 Curling

In the previous subsections we considered a model which even though it is one-dimensional shows properties that are far from being trivial since different switching mechanisms can occur. Many of the findings obtained from this model are relevant for real magnetic nanowires, as long as those are thin enough to be effectively one-dimensional. Nevertheless, for a realistic description of magnetic nanoparticles one needs three-dimensional models and one has to consider the dipole–dipole interaction. In the following we will discuss the degree to which the physics of the switching process changes when one considers a three-dimensional model

including dipole–dipole interaction. Only few numerical results exist so far, some of them we discuss in the following.

Considering the mathematical form of the dipole–dipole interaction in equation (5) one notes that dipoles tend to align, with that trying to build up closed loops or vortices. On the other hand, a loop has an enhanced exchange energy. Therefore to calculate the spin structure of an extended magnetic system is a complicated optimization problem. Even a sufficiently small magnetic nanostructure which, in equilibrium, is in a single-domain state, could reverse its magnetization by more complicated modes than coherent rotation or nucleation. A characteristic length scale below which it is energetically unfavorable for the system to break the long-range order and split into domains is the so-called *exchange length* δ_x (Hubert and Schäfer, 1998). Like the Bloch wall width $\delta = \sqrt{J/2d}$ mentioned earlier, it is a characteristic length scale for a given material. For a spin model it can be derived in the following way: a twist of the direction of the spins by an angle of π over a length scale l (number of spins) costs an exchange energy of

$$\Delta E_x = -J \sum_{i=1}^{l} (1 - \mathbf{S}_i \cdot \mathbf{S}_{i+1})$$

$$\approx -J \sum_{i=1}^{l} \frac{(\theta_i - \theta_{i+1})^2}{2} \approx \frac{J\pi^2}{2l} \qquad (37)$$

assuming constant changes of the angle θ from one spin to the next one (which can also be shown to be the wall profile with the minimum energy by a solution of the corresponding Euler–Lagrange equations). The dipolar field energy of a chain of parallel-oriented dipoles can be expressed via Riemann's ζ function using

$$\zeta(3) = \sum_{i=1}^{\infty} \frac{1}{i^3} \approx 1.202 \qquad (38)$$

Hence, the gain of dipolar energy of a chain of l spins can roughly be estimated to be at most $3wl\zeta(3)$, where $w = \mu_s^2 \mu_0 / 4\pi a^3$ is the strength of the dipole–dipole coupling (see equation (5) and also (Hucht, Moschel and Usadel, 1995) for a similar calculation in two dimensions). A comparison of the energies yields the exchange length (measured as number of atoms)

$$\delta_x = \pi \sqrt{\frac{J}{6\zeta(3)w}} \qquad (39)$$

Note that in a continuum theory the dipolar energy is estimated from formulae for the magnetostatic energy of ellipsoids (Hubert and Schäfer, 1998). The results deviate slightly since the factor $3\zeta(3)$ is replaced by π. We prefer the expression in the preceding text derived directly for a spin model.

Let us now consider a nanowire, that is either a cylindrical system or an extremely elongated ellipsoid. As long as the thickness of the particle is smaller than the exchange length, the magnetization will be homogeneous in the planes perpendicular to the long axis so that the system behaves effectively one-dimensionally (Braun, 1999). For thicknesses larger than the exchange length, reversal modes may occur where the magnetization is nonuniform in the perpendicular planes, for example curling (Aharoni, 1996) (for graphical representations see Nowak, 2001).

The existence of the crossover from nucleation to curling was investigated by simulations of cylindrical systems (Hinzke and Nowak, 2000b; Nowak, 2001). Here, for the first time fast Fourier transformation (FFT) methods for the calculation of the dipolar fields were combined with Monte Carlo simulations with quantified time step. These methods allowed for a statistical investigation of particle sizes of up to 32 768 spins in three dimensions. A systematic numerical determination of the corresponding energy barriers and characteristic times is nevertheless still missing.

5 SIMULATION OF ANTIFERROMAGNETS: EXCHANGE BIAS

For compound materials consisting of an FM in contact with an AFM a shift of the hysteresis loop along the magnetic field axis can occur, which is called *exchange bias* (*EB*). Often, this shift is observed after cooling the entire system in an external magnetic field below the Néel temperature T_N of the AFM. For reviews on EB the reader is referred to the articles by Nogués and Schuller (1999) and Stamps (2000). Although EB has been well known since many years (Meiklejohn and Bean, 1956, 1957) its microscopic origin is still discussed controversially.

A detailed understanding of EB can only be achieved by an understanding of the antiferromagnetic spin structure so that classical spin models are the common starting point for microscopic models of EB. In an early approach by Malozemoff (1987, 1988a,b), EB is attributed to the formation of domain walls in the AFM, perpendicular to the FM/AFM interface due to interface roughness. These domain walls are supposed to occur during cooling in the presence of the magnetized FM and to carry a small net magnetization at the FM/AFM interface (see Figure 4a). This interface magnetization is furthermore supposed to be stable during the reversal of the FM, consequently shifting the hysteresis loop. However, the formation of domain walls in the AFM

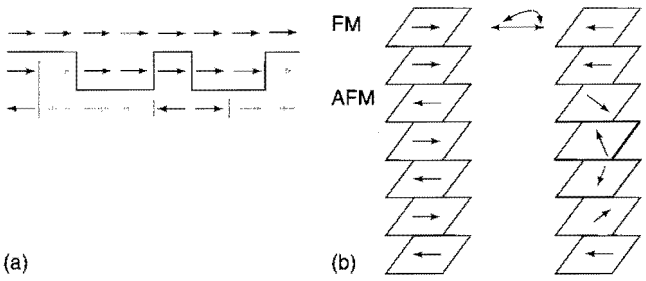

Figure 4. (a) Sketch of the model after Malozemoff (1987, 1988a,b) which shows the FM on top of the AFM in a domain configuration. (b) Sketch of the model Mauri, Siegmann, Bagus and Kay (1987). During reversal of the FM a spring is wound up in the AFM. (Reprinted from *Journal of Magnetism and Magnetic Materials*, Vol 240, 2002, Pages 243–247. Copyright 2002, with permission from Elsevier.)

only due to interface roughness is energetically unfavorable and its occurrence and stability have never been proved.

Alternative approaches have been developed. In a model introduced by Mauri, Siegmann, Bagus and Kay (1987) EB is obtained through a mechanism in which a domain-wall forms in the AFM parallel to the interface while the magnetization of the FM rotates (see Figure 4b). In contrast to experimental findings this mechanism works only for uncompensated interfaces where the interface layer of the AFM is such that is carries a net magnetization. Furthermore the interface is assumed to be perfectly flat since otherwise it would be effectively compensated by roughness. An extension by Koon (1998) for compensated interfaces where the model of Mauri was combined with a spin-flop coupling was later on proved to show no EB (Schulthess and Butler, 1998, 1999). To obtain EB Schulthess and Butler had to assume uncompensated AFM spins at the interface. However, their occurrence and stability during a magnetic hysteresis loop was not explained.

In a recent experiment Miltényi *et al.* (2000) showed that it is possible to strongly influence EB in Co/CoO bilayers by diluting the antiferromagnetic CoO layer, that is by inserting nonmagnetic substitutions ($Co_{1-x}Mg_xO$) or defects ($Co_{1-y}O$) not at the FM/AFM interface but rather throughout the volume part of the AFM. In the same letter in was shown that a corresponding theoretical model, the domain-state (DS) model, investigated by Monte Carlo simulations shows a behavior very similar to the experimental results. It was argued that EB has its origin in a DS in the AFM which triggers the spin arrangement and the FM/AFM exchange interaction at the interface. Later it was shown that a variety of experimental facts associated with EB can be explained within this DS model (Nowak, Misra and Usadel, 2001, 2002; Nowak *et al.*, 2002b; Keller *et al.*, 2002; Misra, Nowak and Usadel, 2003, 2004; Beckmann, Nowak and Usadel, 2003, 2006; Scholten, Usadel and Nowak, 2005; Spray and Nowak, 2006). The importance of defects for the EB effect was also confirmed by experiments on $Fe_xZn_{1-x}F_2$/Co bilayers (Shi, Lederman and Fullerton, 2002) and by experiments (Mewes *et al.*, 2000; Mougin *et al.*, 2001) where it was shown that it is possible to modify EB by means of irradiating an FeNi/FeMn system by He ions in presence of a magnetic field. Depending on the dose of the irradiation and the magnetic field present at the time of irradiation, it was possible to manipulate both the magnitude and even the direction of the EB field. Further support for the relevance of domains in EB systems is given by a direct spectroscopic observation of AFM domains (Nolting *et al.*, 2000; Ohldag *et al.*, 2001). In the following we focus on the DS model.

5.1 Domain-state model

The DS model for EB (Miltényi *et al.*, 2000) consists of t_{FM} monolayers of FM and t_{AFM} monolayers of diluted AFM. The FM is exchange coupled to the topmost layer of the AFM. The geometry of the model is sketched in Figure 5.

The system is described by a classical Heisenberg model with nearest-neighbor exchange on a simple cubic lattice with exchange constants J_{FM} and J_{AFM} for the FM and the AFM respectively, while J_{INT} stands for the exchange constant between FM and AFM. For simplicity we assume that the values of the magnetic moments of FM and AFM are identical (included in the magnetic field energy B). The Hamiltonian of the system is then

$$\begin{aligned}\mathcal{H} = &-J_{\mathrm{FM}} \sum_{\langle i,j \rangle} \boldsymbol{S}_i \cdot \boldsymbol{S}_j - \sum_i \left(d_z S_{iz}^2 + d_x S_{ix}^2 + \boldsymbol{S}_i \cdot \boldsymbol{B} \right) \\ &-J_{\mathrm{AFM}} \sum_{\langle i,j \rangle} \epsilon_i \epsilon_j \boldsymbol{\sigma}_i \cdot \boldsymbol{\sigma}_j - \sum_i \epsilon_i \left(k_z \sigma_{iz}^2 + \boldsymbol{\sigma}_i \cdot \boldsymbol{B} \right) \\ &-J_{\mathrm{INT}} \sum_{\langle i,j \rangle} \epsilon_j \boldsymbol{S}_i \cdot \boldsymbol{\sigma}_j \end{aligned} \tag{40}$$

where $\mathbf{S}_i$ denote normalized spins at sites of the FM layer and $\boldsymbol{\sigma}_i$ denote normalized spins at sites of the AFM.

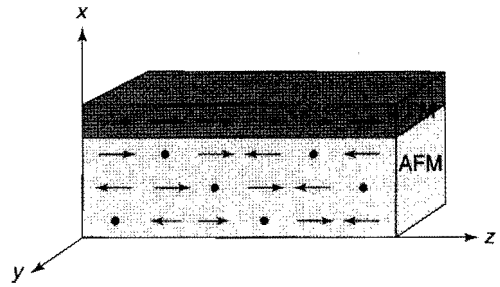

Figure 5. Sketch of the DS model with one FM layer and three diluted AFM layers. The dots mark defects. The easy axis of both FM and AFM is the z axis.

The first line of the Hamiltonian describes the energy of the FM with the z axis as its easy axis (anisotropy constant $d_z > 0$). The dipolar interaction is approximated in the model by an additional anisotropy term (anisotropy constant $d_x = -0.1 J_{\mathrm{FM}}$ in the present case) which includes the shape anisotropy, leading to a magnetization which is preferentially in the y–z plane. The second line is the contribution from the AFM also having its easy axis along z direction. The AFM is diluted, that is a fraction p of sites is left without a magnetic moment ($\epsilon_i = 0$) while the other sites carry a moment ($\epsilon_i = 1$). The last term describes the interaction of the FM with the interface AFM monolayer.

Equation (40) suggests a simple ground state argument for the strength of the bias field. Assuming that all spins in the FM remain parallel during field reversal and that some net magnetization of the interface layer of the AFM remains constant during the reversal of the FM a simple calculation gives the usual estimate for the bias field,

$$t_{\mathrm{FM}} B_{\mathrm{EB}} = J_{\mathrm{INT}} m_{\mathrm{INT}} \tag{41}$$

where m_{INT} is the stable part of the interface magnetization of the AFM (per spin) which is responsible for the EB. For an ideal uncompensated and totally stable interface one would expect $m_{\mathrm{INT}} = 1$. As is well known, this estimate leads to a much too high bias field, while for an ideal compensated interface, on the other hand, one would expect $m_{\mathrm{INT}} = 0$ and, hence, $B_{\mathrm{EB}} = 0$. Experimentally, however, often there is on the one hand no big difference between compensated and uncompensated interfaces and on the other hand, it is found that B_{EB} is much smaller than $J_{\mathrm{INT}}/t_{\mathrm{FM}}$, rather of the order of a few percent of it. The solution of this puzzle is that m_{INT} is neither constant during field reversal nor is it a simple known quantity (Keller *et al.*, 2002; Nowak *et al.*, 2002b) and we discuss this quantity in the following.

5.2 Results from Monte Carlo simulation

Apart from the mean-field work by Scholten, Usadel and Nowak (2005) mainly Monte Carlo methods were used to investigate the DS model. Some of them focused on the Ising limit for the AFM (Nowak, Misra and Usadel, 2001; Nowak *et al.*, 2002b; Beckmann, Nowak and Usadel, 2003, 2006; Spray and Nowak, 2006) while others used the full Heisenberg Hamiltonian of the previous subsection (Nowak, Misra and Usadel, 2002; Misra, Nowak and Usadel, 2003). In the latter case a heat bath algorithm with single-spin-flip dynamics was used where the trial step of the spin update consisted of two steps: firstly a small variation within a cone around the former spin direction, followed, secondly, by a total spin flip. This twofold spin update is ergodic and symmetric and can take care of a broad range of anisotropies, from very soft spins up to the high anisotropy (Ising) limit. To observe the domain structure of the AFM one has to guarantee that typical length scales of the domain structure fit into the system and typical system sizes were a lateral extension of 128×128 and a thickness of $t_{\mathrm{FM}} = 1$ and t_{AFM} ranging from 3 to 9. Periodical boundary conditions were used within the film plane and open boundary conditions perpendicular to it.

The main quantities monitored were the thermal averages of the z component of the magnetic moment for each individual monolayer normalized to the magnetic moment of the saturated monolayer. In simulations the system is first cooled from above to below the ordering temperature of the AFM. During cooling the FM is initially magnetized along the easy z axis resulting in a nearly constant exchange field for the AFM monolayer at the interface. Also, the system is cooled in the presence of an external magnetic field, the cooling field. In addition to the exchange field from the ordered FM this field acts on the AFM also. When the desired final temperature is reached, a magnetic field along the easy axis is applied and reduced in small steps down to a certain minimum value and afterward raised again up to the initial value. This corresponds to one cycle of the hysteresis loop. A hysteresis loop obtained as described in the preceding text is depicted in Figure 6. Results for the magnetization of the

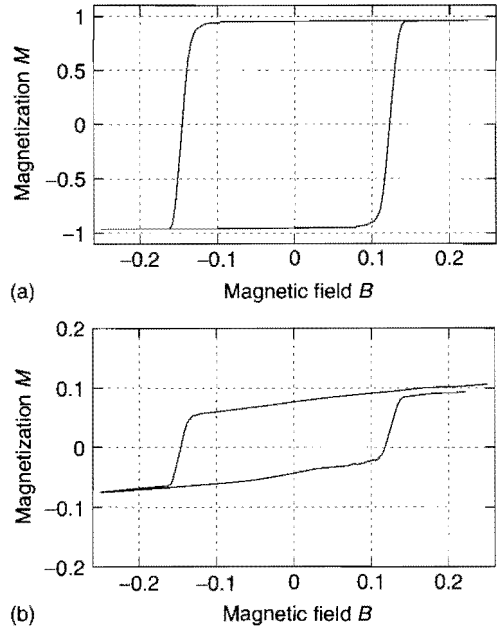

Figure 6. Simulated hysteresis loops of the DS model as explained in the text. Dilution $p = 0.4$, $k_{\mathrm{B}}T = 0.1 J_{\mathrm{FM}}$, positive interface coupling, $J_{\mathrm{INT}} = |J_{\mathrm{AFM}}|$. AFM anisotropy $k_z = J_{\mathrm{FM}}/2$. The cooling field was $B_{\mathrm{c}} = 0.25 J_{\mathrm{INT}}$. The magnetic moment of the FM (a) and the interface monolayer of the AFM (b) normalized to its saturation value is shown. (Reprinted from *Journal of Magnetism and Magnetic Materials*, Vol 240, 2002, Pages 243–247. Copyright 2002, with permission from Elsevier.)

FM (a) as well as that of the AFM interface monolayer (b) are shown. Exchange biasing is clearly observed.

An analysis of the magnetization curve of the interface layer gives an interesting insight into the nature of EB. After the field cooling procedure the AFM interface carries a magnetization. A part of this AFM interface magnetization is stable during hysteresis and leads to the fact that the magnetization curve of the interface layer of the AFM is shifted upward. This irreversible part of the interface magnetization of the AFM acts as an additional effective field on the FM, resulting in EB. Note that the interface magnetization of the AFM also displays hysteresis as a result of the exchange coupling to the FM. This means that the whole interface magnetization of the AFM consists of a reversible part leading to an enhanced coercivity and an irreversible part leading to EB.

In experiments, usually the magnetization of the whole FM/AFM bilayer is measured. The corresponding sample magnetization loop might not only be shifted horizontally but also vertically. The vertical shift contains contributions from the volume part of the AFM as well as from its interface. The volume magnetization of the AFM is induced by the cooling field and hence not shifted when the cooling field is zero and shifted upward when it is finite. The interface contribution depends on the sign of the interface coupling and may be positive, as in our calculation or even negative for negative interface coupling (Nogués, Leighton and Schuller, 2000; Keller *et al.*, 2002; Nowak *et al.*, 2002b).

With the following two sketches we wish to illustrate on a more microscopic basis where the interface magnetization of the AFM comes from, including its partitioning in reversible and irreversible parts. Figure 7(a) shows spin configurations in a small portion of the interface monolayer of the AFM after field cooling. The simulated system size is $64 \times 64 \times 10$ with only one FM monolayer. For simplicity, this simulation was performed in the Ising limit for the AFM ($k_z \to \infty$). The dilution p of the AFM is 50%, nevertheless the spins are much more connected than it appears from the sketch via the third dimension.

Obviously, the AFM is in a DS, where a domain is defined as a region of undisturbed antiferromagnetic order. The reason for the domain formation and, consequently, for the lack of long-range order is the interface magnetization which couples to the exchange field coming from the FM and the external field (both pointing up) lowering the energy of the system. The interface magnetization follows from two contributions. Examples for both are indicated via the circles. One contribution comes from parallel spin pairs in the domain walls (*domain-wall magnetization*), all pointing up in our example (Figure 7a), that is, into the direction of the exchange field of the FM and the external field. A second contribution comes from an imbalance of the number of defects of the two antiferromagnetic sublattices

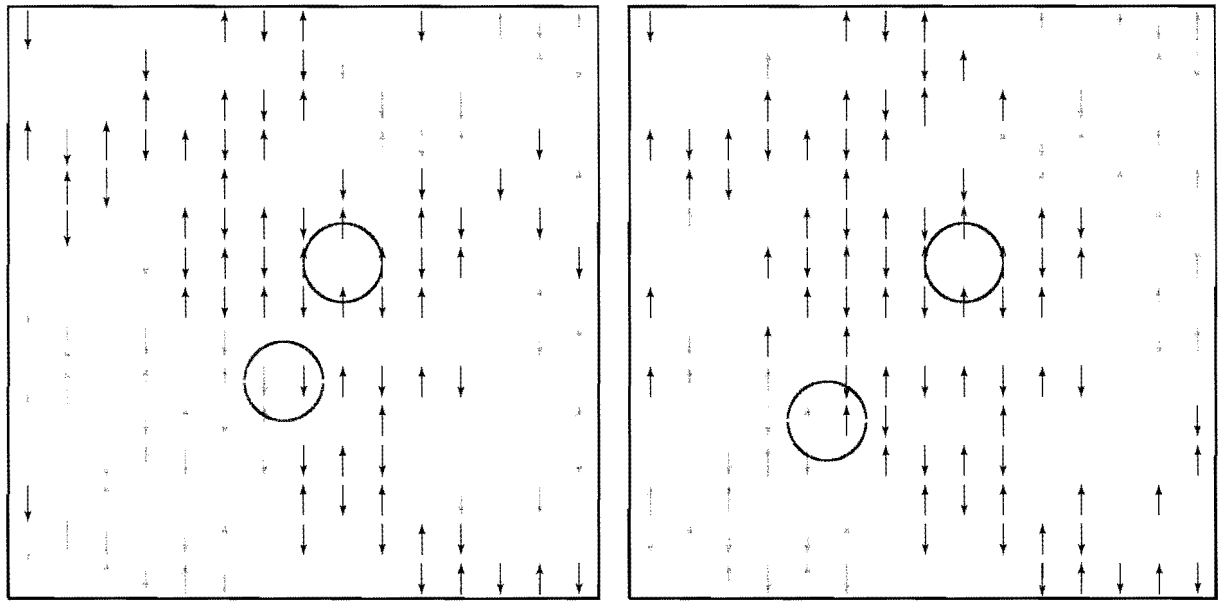

(a) (b)

Figure 7. Snapshots of spin configurations in a small portion of the interface monolayer of the AFM after field cooling with the external field and the FM magnetization pointing upward (a) and after reversal of the FM (b). The interface coupling is assumed to be positive. The gray shading distinguishes different AFM domains. The circles mark sources of magnetization, wall magnetization as well as volume magnetization.

(*volume magnetization*). The imbalance of the number of defects of the two antiferromagnetic sublattices also leads to a net magnetization within a domain which couples to the exchange field of the FM and the external field. The reason for the imbalance is that the domain structure is not random. Rather, it is an optimized structure arising during the initial cooling procedure with as much magnetization as possible coupling to the exchange field of the FM and the external field, following the energy minimization principle.

However, an AFM interface magnetization alone cannot lead to EB. Only the irreversible part of it (during hysteresis) may lead to EB. Figure 7(b) shows, for comparison, spin configurations in the same portion of the interface monolayer of the AFM after reversal of the FM. Clearly, the major part of the domain structure did not change during reversal of the FM. However, there are rearrangements on smaller length scales, leading mainly to the fact that the domain-wall magnetization changes its sign. In Figure 7(b) all of the spin pairs within domain walls are pointing down following the reversed FM and the external field.

However, the volume magnetization coming from the defects remains frozen. The stability of the domain structure stems from the fact that the domain walls are pinned at defects sites as well as between pairs of spins which are aligned with the field. Hence, during a movement of the domain-wall energy barriers may have to be overcome by thermal activation. This explains why a large domain in general will stay in a metastable state on exponentially long timescales, while rearrangements on a shorter length scale are possible, of course depending on the temperature and the material parameters of the AFM.

Many of the essential properties of diluted AFMs, the occurrence of DSs, metastability, remnant magnetization, and slow relaxation, among others, have been investigated before, even though not in the context of EB (for reviews on diluted AFMs see Kleemann, 1993; Belanger, 1998, for a detailed discussion of the connection between diluted AFMs and EB systems see Nowak *et al.*, 2002b).

Important features of EB systems found experimentally (Keller *et al.*, 2002) have their counterpart in the simulations (Nowak *et al.*, 2002b), such as the order of magnitude of EB fields, the shape of hysteresis curves, the dilution dependence of EB, its temperature dependence, the training effect, and the occurrence of positive EB. Other properties of EB systems, which were successfully investigated within the framework of the DS model are the dependence of EB on thickness of the AFM (Nowak, Misra and Usadel, 2001; Ali *et al.*, 2003), the dependence on the anisotropy of the AFM in Nowak, Misra and Usadel (2002), the influence of ion irradiation (Misra, Nowak and Usadel, 2003) asymmetric reversal modes (Beckmann, Nowak and Usadel, 2003), properties of the AFM domain structures (Misra, Nowak and Usadel, 2004), the enhanced coercivity (Scholten, Usadel and Nowak, 2005), the cooling field dependence (Beckmann, Nowak and Usadel, 2003), and the influence of interface roughness (Spray and Nowak, 2006). However, finally one should note that most of the AFMs used in EB systems have a polycrystalline structure (Stiles and McMichael, 1999; Suess *et al.*, 2003), which so far was not taken into account by the DS model. Work following these lines is still missing and would certainly contribute to the further understanding of EB.

6 CONCLUSIONS AND OUTLOOK

Within the framework of classical spin models it is possible to investigate magnetic properties of a variety of different materials, as for example, ferri-, ferro-, or antiferromagnets, and even heterostructures composed of several different materials. Simulation techniques for the investigation of thermal equilibrium properties exist and – to some extent – also for nonequilibrium situations.

However, classical spin models neglect quantum effects and, furthermore, one expects certain limits for the validity of the stochastic LLG equation regarding its short-time spin dynamics as well as the form of the damping which still suffers from a lack of microscopic understanding. A mathematical formulation of damping (Smith and Arnett, 2001; Safonov and Bertram, 2002; Rebei and Parker, 2003) as well as a systematic construction and parameterization of classical spin model Hamiltonians (Mryasov, Nowak, Guslienko and Chantrell, 2005) for certain given materials on the basis of first-principles calculation remain a challenge for current research.

NOTE

[1] The fact that the noise is multiplicative in the LLG equation has been questioned, since the parameter space is the unit sphere, so that the relevant random-field term (giving rise to a torque) and the magnetization derivative are restricted to the tangent plane. The use of a Heun scheme might thus not be mandatory.

REFERENCES

Aharoni, A. (1969). Effect of a magnetic field on the superparamagnetic relaxation time. *Physical Review*, **177**, 793.

Aharoni, A. (1996). Comment on Kramer's rate theory, broken symmetries, and magnetization reversal. *Journal of Applied Physics*, **80**, 3133.

Ali, M., Marrows, C.H., Al-Jawad, M., *et al.* (2003). Antiferromagnetic layer thickness dependence of the IrMnCo exchange bias system. *Physical Review B*, **68**, 214420.

Anderson, P.W. (1963). Exchange in insulators: superexchange, direct exchange, and double exchange. In *Magnetism: A Treatise on Modern Theory and Materials*, Rado, G.T. and Suhl, H. (Eds.), Academic Press: New York, Vol. 1.

Becker, R. and Döring, W. (1935). Kinetische Behandlung der Keimbildung in übersättigten Dämpfen. *Annalen der Physik (Leipzig)*, **24**, 719.

Beckmann, B., Nowak, U. and Usadel, K.D. (2003). Asymmetric reversal modes in ferromagnetic/antiferromagnetic multilayers. *Physical Review Letters*, **91**, 187201.

Beckmann, B., Usadel, K.D. and Nowak, U. (2006). Cooling field dependence of asymmetric reversal modes for ferromagnetic/antiferromagnetic multilayers. *Physical Review B*, **74**, 054431.

Belanger, D.P. (1998). Experiments on the random field Ising model. In *Spin Glasses and Random Fields*, Young, A.P. (Ed.), World Scientific: Singapore.

Berkov, D.V. (2007). Magnetization dynamics including thermal fluctuations. In *Handbook of Magnetism and Advanced Magnetic Materials*, Kronmüller, H. and Parkin, S. (Eds.), John Wiley & Sons: Chichester, Vol. 2.

Berkov, D.V., Ramstöck, K.R. and Hubert, A. (1993). Solving micromagnetic problems. *Physica Status Solidi A*, **137**, 207.

Binder, K. and Heermann, D.W. (1997). *Monte Carlo Simulation in Statistical Physics*, Springer-Verlag: Berlin.

Braun, H.B. (1993). Thermally activated magnetization in elongated ferromagnetic particles. *Physical Review Letters*, **71**, 3557.

Braun, H.B. (1994a). Fluctuations and instabilities of ferromagnetic domain-wall pairs in an external magnetic field. *Physical Review B*, **50**, 16485.

Braun, H.B. (1994b). Kramer's rate theory, broken symmetries, and magnetization reversal. *Journal of Applied Physics*, **76**, 6310.

Braun, H.B. (1999). Nucleation in ferromagnetic nanowires – magnetostatics and topology. *Journal of Applied Physics*, **85**, 6172.

Braun, H.B. (2000). Stochastic magnetization dynamics in magnetic nanostructures: from Néel-Brown to soliton-antisoliton creation. In *Structure and Dynamics of Heterogenous Systems*, Entel, P. and Wolf, D.E. (Eds.), World Scientific: Singapore.

Brown, W.F. (1963a). *Micromagnetics*, John Wiley & Sons: New York.

Brown, W.F. (1963b). Thermal fluctuations of a single-domain particle. *Physical Review*, **130**, 1677.

Chang, T., Zhu, J-G. and Judy, J.H. (1993). Method for investigating the reversal properties of isolated barium ferrite fine particles utilizing MFM. *Journal of Applied Physics*, **73**, 6716.

Chantrell, R.W., Lyberatos, A. and Wohlfarth, E. (1986). The coefficient of magnetic viscosity II: the time dependent magnetisation of interacting fine particle materials. *Journal of Physics F*, **16**, L145.

Chantrell, R.W., Walmsley, N., Gore, J. and Maylin, M. (2000). Calculation of the susceptibility of interacting superparamagnetic particles. *Physical Review B*, **63**, 024410.

Cheng, X.Z., Jalil, M.B.A., Lee, H.K. and Okabe, Y. (2006). Mapping the Monte Carlo scheme to Langevin dynamics: a Fokker-Planck approach. *Physical Review Letters*, **96**, 067208.

Chubykalo, O., Nowak, U., Chantrell, R.W. and Garanin, D. (2006). Dynamic approach for micromagnetics close to the Curie temperature. *Physical Review B*, **74**, 094436.

Chubykalo, O., Nowak, U., Smirnov-Rueda, R., *et al.* (2003a). The Monte Carlo technique with quantified time step: application to the motion of magnetic moments. *Physical Review B*, **67**, 64422.

Chubykalo, O., Smirnov-Rueda, R., Wongsam, M.A., *et al.* (2003b). Brownian dynamics approach to interacting magnetic moments. *Journal of Magnetism and Magnetic Materials*, **266**, 28.

Coffey, W.T. (1996). *The Langevin Equation*, World Scientific: Singapore.

Coffey, W.T., Crothers, D.S.F., Dorman, J.L., *et al.* (1998a). Effect of an oblique magnetic field on the superparamagnetic relaxation time. II. Influence of the gyromagnetic term. *Physical Review B*, **58**, 3249.

Coffey, W.T., Crothers, D.S.F., Dorman, J.L., *et al.* (1998b). Range of validity of Kramer's escape rates for non-axially symmetric problems in superparamagnetic relaxation. *Journal of Physics: Condensed Matter*, **10**, 9093.

Coffey, W.T., Crothers, D.S.F., Dorman, J.L., *et al.* (1998c). Thermally activated relaxation time of a single domain ferromagnetic particle subjected to a uniform field at an oblique angle to the easy axis: comparison with experimental observations. *Physical Review Letters*, **80**, 5655.

Ettelaie, R. and Moore, M.A. (1984). Comparison of Langevin and Monte Carlo dynamics. *Journal of Physics A: Mathematical and General*, **17**, 3505.

Garanin, D.A. (1991). Dynamics of elliptic domain walls. *Physica A*, **178**, 467.

Garanin, D.A. (1997). Fokker-Planck and Landau-Lifshitz-Bloch equation for classical ferromagnets. *Physical Review B*, **55**, 3050.

García-Palacios, J.L. and Lázaro, F.J. (1998). Langevin-dynamics study of the dynamical properties of small magnetic particles. *Physical Review B*, **58**, 14937.

García-Palacios, J.L. and Svedlindh, P. (2000). Langevin-dynamics study of the dynamical properties of small magnetic particles. *Physical Review Letters*, **85**, 3724.

Gilbert, T.L. (1955). A Lagrangian formulation of the gyromagnetic equation of the magnetization field. *Physical Review*, **100**, 1243.

Glauber, R.J. (1963). Time-dependent statistics of the Ising model. *Journal of Mathematical Physics*, **2**, 294.

Greiner, A., Strittmatter, W. and Honerkamp, J. (1988). Numerical integration of stochastic differential equation. *Journal of Statistical Physics*, **51**, 95.

Heisenberg, W. (1928). Zur Theorie des Ferromagnetismus. *Zeitschrift fur Physik*, **49**, 619.

Hinzke, D. and Nowak, U. (1998). Magnetization switching in a Heisenberg model for small ferromagnetic particles. *Physical Review B*, **58**, 265.

Hinzke, D. and Nowak, U. (1999). Monte Carlo simulation of magnetization switching in a Heisenberg model for small ferromagnetic particles. *Computer Physics Communications*, **121–122**, 343.

Hinzke, D. and Nowak, U. (2000a). Magnetic relaxation in a classical spin chain as model for nanowires. *Physical Review B*, **61**, 6734.

Hinzke, D. and Nowak, U. (2000b). Magnetization switching in nanowires: Monte Carlo study with fast Fourier transformation for dipolar fields. *Journal of Magnetism and Magnetic Materials*, **221**, 365.

Hinzke, D., Nowak, U. and Usadel, K.D. (2000). Thermally activated magnetization reversal in classical spin chains. In *Structure and Dynamics of Heterogenous Systems*, Entel, P. and Wolf, D.E. (Eds.), World Scientific: Singapore.

Hubert, A. and Schäfer, R. (1998). *Magnetic Domains*, Springer-Verlag: Berlin.

Hucht, A., Moschel, A. and Usadel, K.D. (1995). Monte-Carlo study of the reorientation transition in Heisenberg models with dipolar interaction. *Journal of Magnetism and Magnetic Materials*, **148**, 32.

Kazantseva, N., Wieser, R. and Nowak, U. (2005). Transition to linear domain walls in nanoconstrictions. *Physical Review Letters*, **94**, 37206.

Keller, J., Miltényi, P., Beschoten, B., *et al.* (2002). The domain state model for exchange bias II: experiment. *Physical Review B*, **66**, 14431.

Kirby, R.D., Shen, J.X., Hardy, R.J. and Sellmyer, D.J. (1994). Magnetization reversal in nanoscale magnetic films with perpendicular anisotropy. *Physical Review B*, **49**, 10810.

Kleemann, W. (1993). Random-field induced antiferromagnetic, ferroelectric and structural domains states. *International Journal of Modern Physics B*, **7**, 2469.

Koon, N.C. (1998). Calculations of exchange bias in thin films with ferromagnetic/antiferromagnetic interfaces. *Physical Review Letters*, **78**, 4865.

Landau, D.L. and Lifshitz, E. (1935). On the theory of the dispersion of magnetic permeability in ferromagnetic bodies. *Physikalische Zeitschrift der Sowjetunion*, **8**, 153.

Levy, L-P. (2000). *Magnetism and Superconductivity*, Springer-Verlag: Berlin.

Lyberatos, A., Berkov, D.V. and Chantrell, R.W. (1993). A method for the numerical simulation of the thermal magnetization fluctuations in micromagnetics. *Journal of Physics: Condensed Matter*, **5**, 8911.

Lyberatos, A. and Chantrell, R.W. (1993). Thermal fluctuations in a pair of magnetostatistically coupled particles. *Journal of Applied Physics*, **73**, 6501.

Lyberatos, A., Earl, J. and Chantrell, R.W. (1996). Model of thermally activated magnetization reversal in rare-earth-transition-metal compounds. *Physical Review B*, **53**, 5493.

Malozemoff, A.P. (1987). Random-field model of exchange anisotropy at rough ferromagnetic-antiferromagnetic interfaces. *Physical Review B*, **35**, 3679.

Malozemoff, A.P. (1988a). Heisenberg-to-Ising crossover in a random-field model with uniaxial anisotropy. *Physical Review B*, **37**, 7673.

Malozemoff, A.P. (1988b). Mechanism of exchange anisotropy. *Journal of Applied Physics*, **63**, 3874.

Mauri, D., Siegmann, H.C., Bagus, P.S. and Kay, E. (1987). Simple model for thin ferromagnetic films exchange coupled to an antiferromagnetic substrate. *Journal of Applied Physics*, **62**, 3047.

Meiklejohn, W.H. and Bean, C.P. (1956). New magnetic anisotropy. *Physical Review*, **102**, 1413.

Meiklejohn, W.H. and Bean, C.P. (1957). New magnetic anisotropy. *Physical Review*, **105**, 904.

Mewes, T., Lopusnik, R., Fassbender, J., *et al.* (2000). Suppression of exchange bias by ion irradiation. *Applied Physics Letters*, **76**, 1057.

Miltényi, P., Gierlings, M., Keller, J., *et al.* (2000). Diluted antiferromagnets in exchange bias: Proof of domain state model. *Physical Review Letters*, **84**, 4224.

Misra, A., Nowak, U. and Usadel, K.D. (2003). Control of exchange bias by diluting the antiferromagnetic layer. *Journal of Applied Physics*, **93**, 6593.

Misra, A., Nowak, U. and Usadel, K.D. (2004). Structure of domains in an exchange bias model. *Journal of Applied Physics*, **95**, 1357.

Mougin, A., Mewes, T., Jung, M., *et al.* (2001). Local manipulation and reversal of the exchange bias field by ion irradiation in FeNi/FeMn double layers. *Physical Review B*, **63**, 60409.

Mryasov, O.N., Nowak, U., Guslienko, K. and Chantrell, R.W. (2005). Temperature dependent magnetic properties of FePt: effective spin Hamiltonian model. *Europhysics Letters*, **69**, 805.

Nogués, J., Leighton, C. and Schuller, I.K. (2000). Correlation between antiferromagnetic interface coupling and positive exchange bias. *Physical Review B*, **61**, 1315.

Nogués, J. and Schuller, I.K. (1999). Exchange bias. *Journal of Magnetism and Magnetic Materials*, **192**, 203.

Nolting, F., Scholl, A., Stöhr, J., *et al.* (2000). Direct observation of the alignment of ferromagnetic spins by antiferromagnetic spins. *Nature*, **405**, 767.

Nowak, U. (1997). Micromagnetic simulation of nanoscale films with perpendicular anisotropy. *Journal of Applied Physics*, **81**, 5579.

Nowak, U. (2001). Thermally activated reversal in magnetic nanostructures. In *Annual Reviews of Computational Physics IX*, Stauffer, D. (Ed.), World Scientific: Singapore, p. 105.

Nowak, U., Chantrell, R.W. and Kennedy, E.C. (2000). Monte Carlo simulation with time step quantification in terms of Langevin dynamics. *Physical Review Letters*, **84**, 163.

Nowak, U., Heimel, J., Kleinefeld, T. and Weller, D. (1997). Domain dynamics of magnetic films with perpendicular anisotropy. *Physical Review B*, **56**, 8143.

Nowak, U., Misra, A. and Usadel, K.D. (2001). Domain state model for exchange bias. *Journal of Applied Physics*, **89**, 7269.

Nowak, U., Misra, A. and Usadel, K.D. (2002). Modeling exchange bias microscopically. *Journal of Magnetism and Magnetic Materials*, **240**, 243.

Nowak, U., Mryasov, O.N., Wieser, R., *et al.* (2005). Spin dynamics of magnetic nanoparticles: beyond Brown's theory. *Physical Review B*, **72**, 172410.

Nowak, U., Rüdiger, U., Fumagalli, P. and Güntherodt, G. (1996). Dependence of magnetization reversal on the crystallite size in

MnBi thin films: experiment, theory, and computer simulation. *Physical Review B*, **54**, 13017.

Nowak, U., Usadel, K.D., Miltényi, P., *et al.* (2002). The domain state model for exchange bias I: theorie. *Physical Review B*, **66**, 14430.

Ohldag, H., Scholl, A., Nolting, F., *et al.* (2001). Spin reorientation at the antiferromagnetic NiO(001) surface in response to an adjacent ferromagnet. *Physical Review Letters*, **86**, 2878.

Rebei, A. and Parker, G. (2003). Fluctuation and dissipation of coherent magnetization. *Physical Review B*, **67**, 104434.

Reif, F. (1965). *Fundamentals of Statistical and Thermal Physics*, McGraw-Hill Book Company: New York.

Rikvold, P.A. and Gorman, B.M. (1994). Recent results on the decay of metastable phases. In *Annual Reviews of Computational Physics I*, Stauffer, D. (Ed.), World Scientific: Singapore, p. 149.

Rikvold, P.A., Tomita, H., Miyashita, S. and Sides, S.W. (1994). Metastable lifetimes in a kinetic Ising model: dependence on field and system size. *Physical Review E*, **49**, 5080.

Safonov, V. and Bertram, N. (2002). Thermal magnetization noise in a thin film. *Physical Review B*, **65**, 172417.

Schneider, C.M. and Blügel, S. (Eds.) (2005). *Magnetism Goes Nano*. Lecture Notes of the 36th Spring School of the IFF Jülich, Forschungs-zentrum Jülich GmbH: Jülich.

Scholten, G., Usadel, K.D. and Nowak, U. (2005). Coercivity and exchange bias of ferromagnetic/antiferromagnetic multilayers. *Physical Review B*, **71**, 64413.

Schulthess, T.C. and Butler, W.H. (1998). Consequences of spin-flop coupling in exchange biased films. *Physical Review Letters*, **81**, 4516.

Schulthess, T.C. and Butler, W.H. (1999). Coupling mechanisms in exchange biased films. *Journal of Applied Physics*, **85**, 5510.

Shi, H.T., Lederman, D. and Fullerton, E.E.C. (2002). Exchange bias in $Fe_xZn_{1-x}F_2$/Co bilayers. *Journal of Applied Physics*, **91**, 7763.

Smirnov-Rueda, R., Chubykalo, O., Nowak, U., *et al.* (2000). Real time quantification of Monte Carlo steps for different time scales. *Journal of Applied Physics*, **87**, 4798.

Smirnov-Rueda, R., Hannay, J.D., Chubykalo, O., *et al.* (1999). Simulation of magnetic relaxation by a Monte Carlo technique with correlations and quantified time steps. *IEEE Transactions on Magnetics*, **35**, 3730.

Smith, N. and Arnett, P. (2001). White-noise magnetization fluctuations in magnetoresistive heads. *Applied Physics Letters*, **78**, 1448.

Spray, J. and Nowak, U. (2006). Exchange bias in ferromagnetic/antiferromagnetic bilayers with imperfect interfaces. *Journal of Physics D*, **39**, 4536.

Stamps, R.L. (2000). Mechanisms for exchange bias. *Journal of Physics D*, **33**, R247.

Stauffer, D., Hehl, F.W., Winkelmann, V. and Zabolitzky, J.G. (1993). *Computer Simulation and Computer Algebra*, Springer-Verlag: Berlin.

Steevens, K.W.H. (1963). Spin hamiltonians. In *Magnetism: A Treatise on Modern Theory and Materials*, Rado, G.T. and Suhl, H. (Eds.), Academic Press: New York, Vol. 1.

Stiles, M.D. and McMichael, R.D. (1999). Model for exchange bias in polycrystalline ferromagnet-antiferromagnet bilayers. *Physical Review B*, **59**, 3722.

Suess, D., Kirschner, M., Schrefl, T., *et al.* (2003). Exchange bias of polycrystalline antiferromagnets with perfectly compensated interfaces. *Physical Review B*, **67**, 54419.

Swendsen, R.H. and Wang, J.S. (1987). Nonuniversal critical dynamics in Monte Carlo simulations. *Physical Review Letters*, **58**, 86.

Vedmedenko, E.Y., Kubetzka, A., von Bergmann, K., *et al.* (2004). Domain wall orientation in magnetic nanowires. *Physical Review Letters*, **92**, 077207.

Verdes, C., Ruiz-Diaz, B., Thompson, S., *et al.* (2002). Computational model of the magnetic and transport properties of interacting fine particles. *Physical Review B*, **65**, 174417.

Vesely, F. (1993). *Computational Physics*, Universitätsverlag: Wien.

Wagner, D. (1972). *Introduction to the Theory of Magnetism*, Pergamon Press: Oxford.

Wernsdorfer, W., Doudin, B., Mailly, D., *et al.* (1996a). Nucleation of magnetization reversal in individual nanosized nickel wires. *Physical Review Letters*, **77**, 1873.

Wernsdorfer, W., Hasselbach, K., Sulpice, A., *et al.* (1996b). Dynamical measurement of domain-wall nucleation and annihilation in individual amorphous Co particles. *Physical Review B*, **53**, 3341.

Wernsdorfer, W., Hasselbach, K., Benoit, A., *et al.* (1997a). Measurements of magnetization switching in individual nickel nanowires. *Physical Review B*, **55**, 11552.

Wernsdorfer, W., Orozco, E.B., Hasselbach, K., *et al.* (1997b). Experimental evidence of the Néel-Brown model of magnetization reversal. *Physical Review Letters*, **78**, 1791.

Wieser, R., Nowak, U. and Usadel, K.D. (2004). Domain wall mobility in nanowires: transverse vs. vortex walls. *Physical Review B*, **69**, 64401.

Wieser, R., Usadel, K.D. and Nowak, U. (2006). Thermodynamic behavior of nano-magnets with vortex configuration. *Physical Review B*, **74**, 094410.

Wolf, D.E. (1998). Stochastic differential equations. In *Advances in Computer Simulation*, Kondor, I. and Kertész, J. (Eds.), Springer: Heidelberg, p. 104.

Wolff, U. (1989). Collective Monte Carlo updating for spin systems. *Physical Review Letters*, **62**, 361.